

Supplementary Information

Evaporating Potential in Conical PTFE Membrane with Asymmetric Electrodes

Zheng Liu ¹, Ting Chen ^{2*}, Qingshang Wang ¹, Guohua Liu ^{1*}

¹ Beijing Key Laboratory of Multiphase Flow and Heat Transfer for Low Grade Energy Utilization, North China Electric Power University, Beijing 102206, PR China

² School of Optoelectronic Materials and Technology, Jianghan University, Wuhan 430056, China

*Corresponding author. E-mail address: chenting631@163.com,
liuguohua126@126.com

Simulation section

The velocity distribution for three type structures are numerically calculated using the finite-element software package COMSOL Multiphysics. For steady fluidic flow of porous material, it is determined by Brinkman equation:

$$-\nabla p + \nabla \cdot (\mu \frac{1}{\varepsilon_p} \nabla \mathbf{u} - \frac{2}{3} \mu \frac{1}{\varepsilon_p} (\nabla \cdot \mathbf{u}) \mathbf{I}) - (\mu \kappa^{-1} + \frac{Q_m}{\varepsilon_p^2}) \mathbf{u} = 0 \quad (1)$$

$$-\nabla \cdot \mathbf{u} = Q_m \quad (2)$$

where p is fluidic pressure, \mathbf{u} is flow velocity, μ is fluidic viscosity, ε_p is porosity κ is permeability, Q_m is the mass source. For boundary conditions, the bottom is the fluid inlet and the top is the fluid outlet.

To simulate the energy conversion inside the channel, the electrostatic field, ions concentration and the velocity fields can be determined by coupled Poisson–Nernst–Planck (PNP) equations and Navier–Stocks (N-S) equation:

$$-\nabla \cdot (\varepsilon_0 \varepsilon_f \nabla \phi) = F \sum_{i=1}^2 z_i c_i \quad (3)$$

$$-\nabla \cdot (\varepsilon_0 \varepsilon_m \nabla \phi) = 0 \quad (4)$$

$$\mathbf{J}_i = c_i \mathbf{u} - D_i \nabla c_i - \frac{D_i z_i F c_i}{R T} \nabla \phi \quad (5)$$

$$-\nabla \cdot \mathbf{J}_i = 0 \quad (6)$$

$$-\nabla p + \nabla \cdot (\mu \nabla \mathbf{u}) - F \sum_{i=1}^2 z_i c_i \nabla \phi = 0 \quad (7)$$

$$-\nabla \cdot \mathbf{u} = 0 \quad (8)$$

where ε_0 , ε_f and ε_m is the absolute permittivity of vacuum, fluid relative permittivity and membrane relative permittivity, respectively. F , z , D , R , T , μ is the Faraday constant, ions valence, diffusion coefficient, gas constant, temperature, fluid viscosity,

respectively. The ϕ , c_i , \mathbf{u} , p is the potential, ions concentration, fluid velocity and pressure, respectively. At the channel entrance, the velocity and ion concentration (1e-7 mol/L for DI water) is specified. The wall surface charge is fixed at 5 mC/m², impermeable to ions and no-slip condition. The channel outlet pressure is 0.

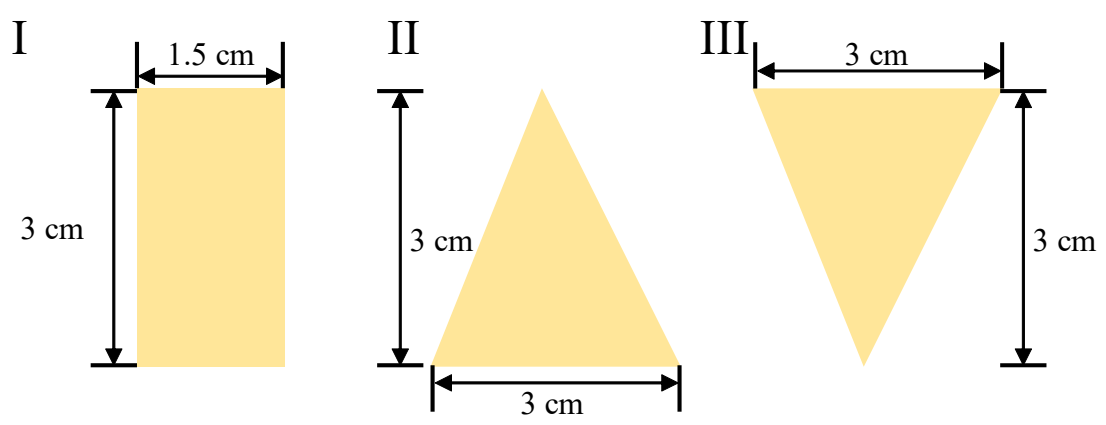


Fig. S1 The geometric schematics of the three types of generators.

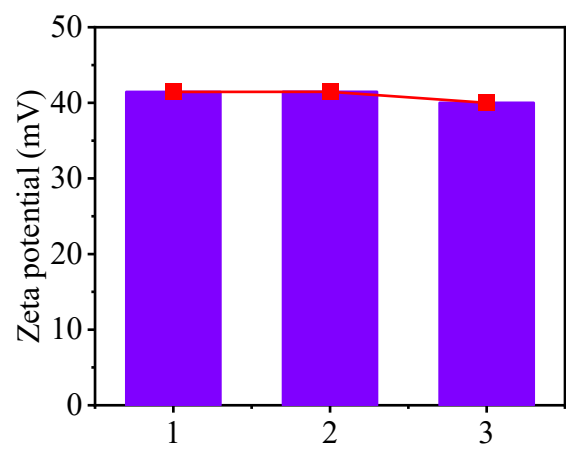


Fig. S2. The zeta potential under three measurements.

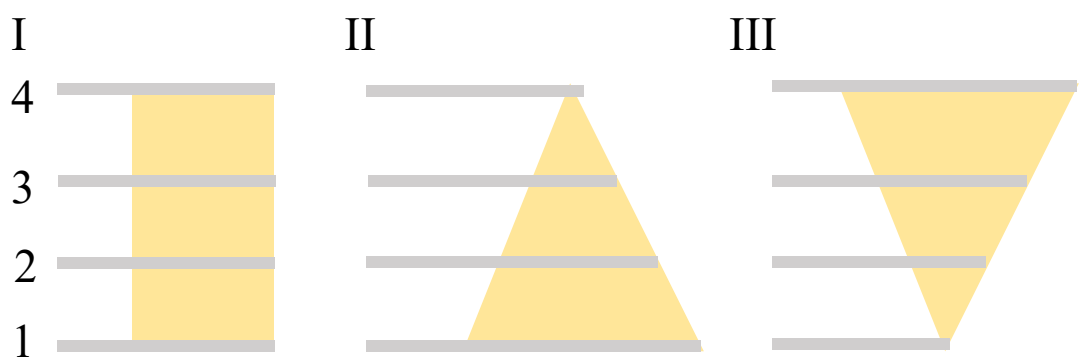


Fig. S3. The diagram of multi-electrode arrangement.

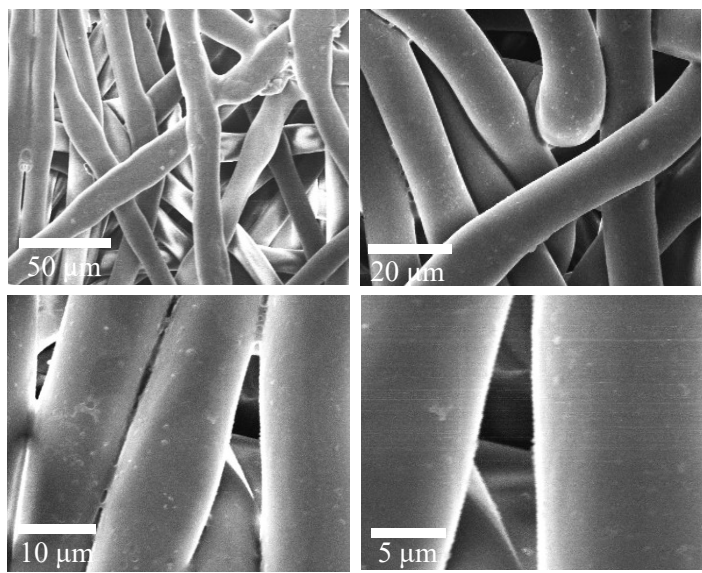


Fig. S4 The SEM mages of PTFE membranes.

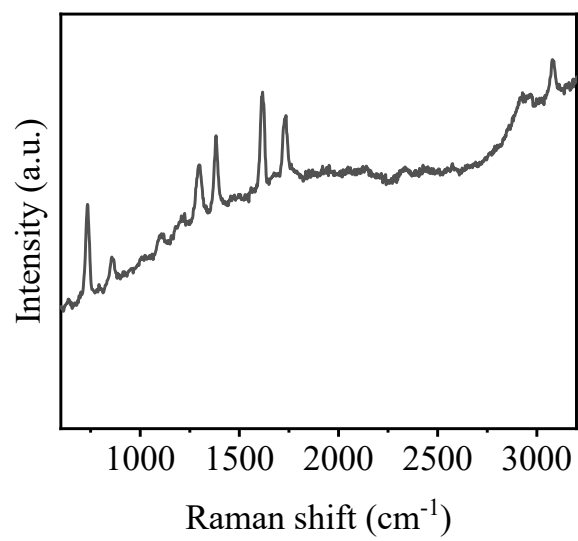


Fig. S5 The Raman spectra of membrane.

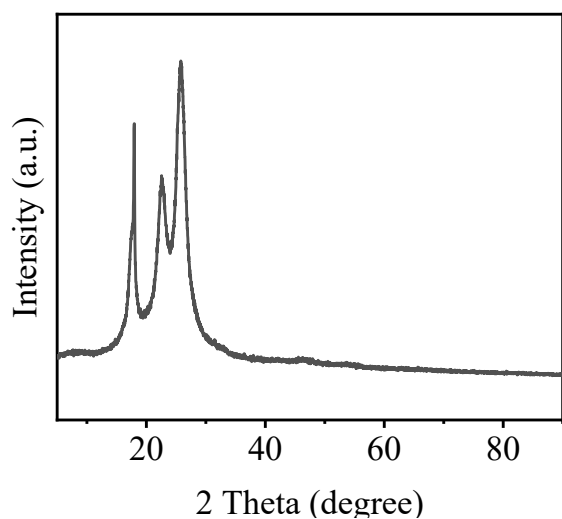


Fig. S6 The XRD pattern of membrane.

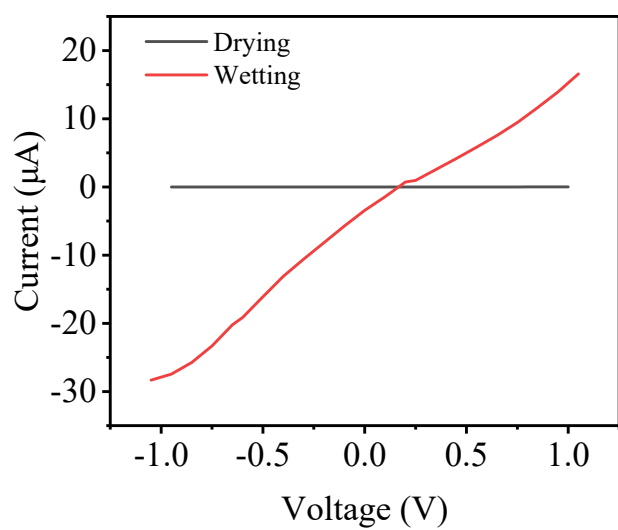


Fig. S7 The IV curves of drying and wetting PTFE membranes.

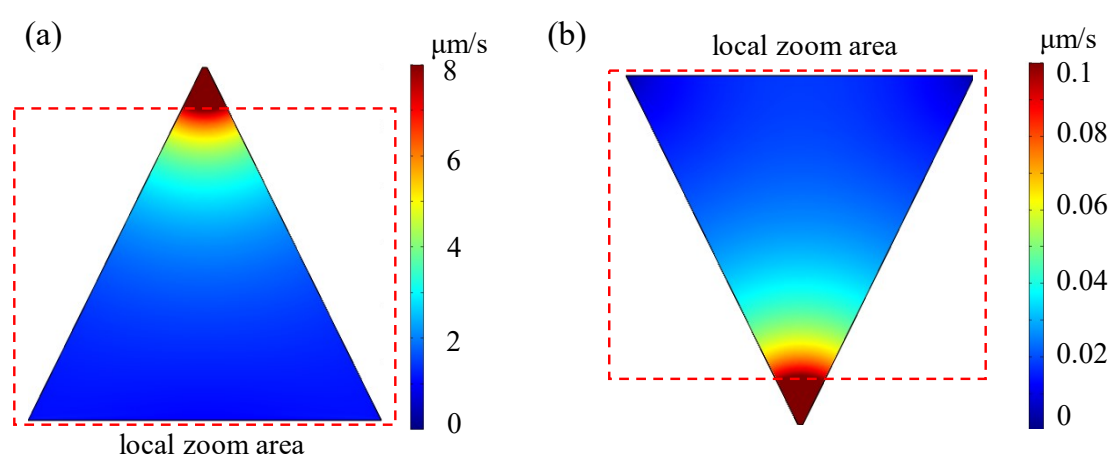


Fig. S8 The local zoomed-in image of (a) FCS and (b) RCS.

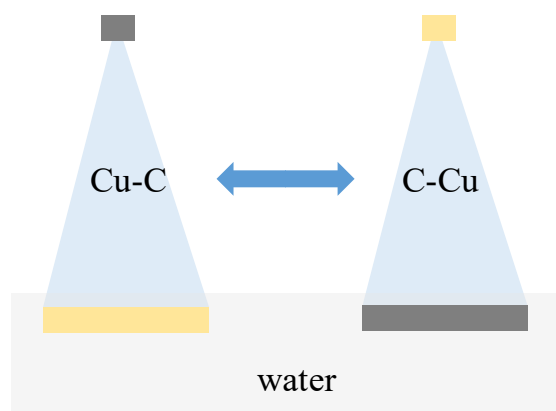


Fig. S9 The diagram of generator upon Cu-C and C-Cu electrodes.

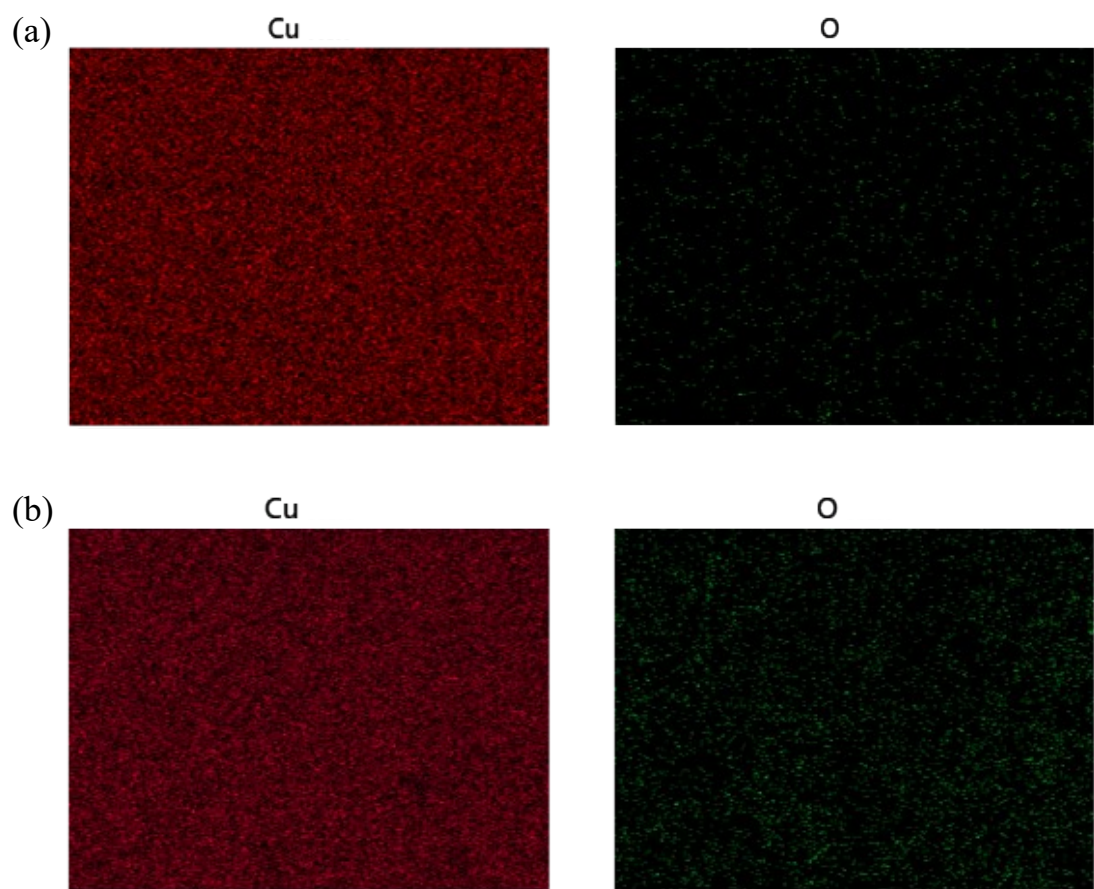


Fig. S10 EDS images of Cu electrode before (a) and after (b) measurement in DI water.

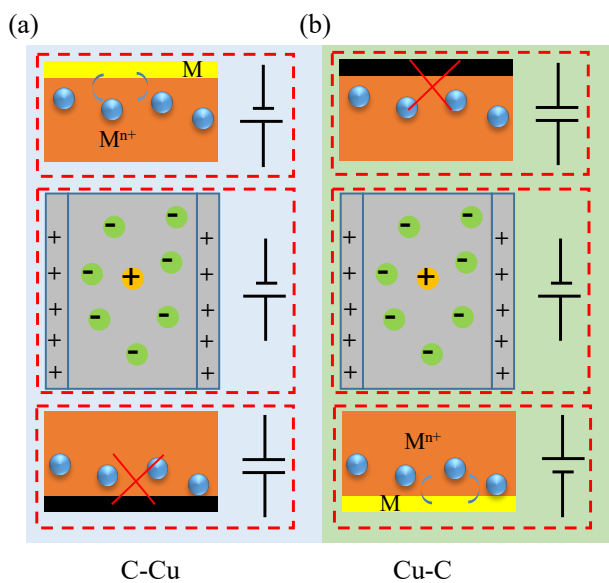


Fig. S11 The mechanism analysis for (a) asymmetric Cu-C electrodes (d) asymmetric C-Cu generator.

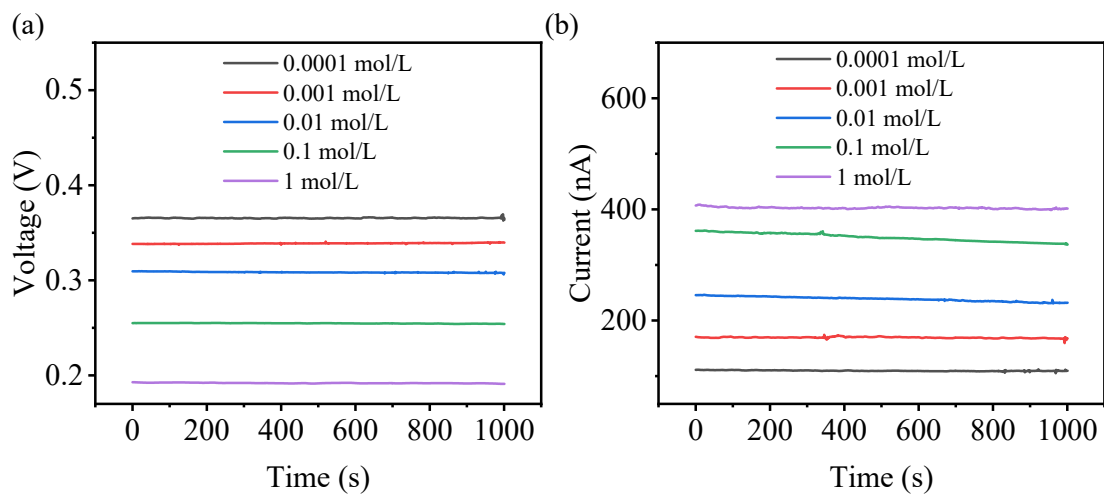


Fig. S12 (a) The open circuit voltage and (b) short circuit current under different ion concentration. (c) The open circuit voltage and short circuit current as a function of ion concentration.

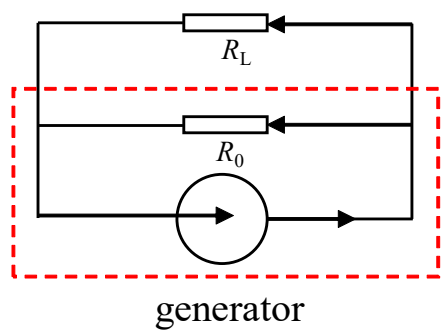


Fig. S13 The equivalent circuit diagram of evaporating-hydrovoltaic generator.

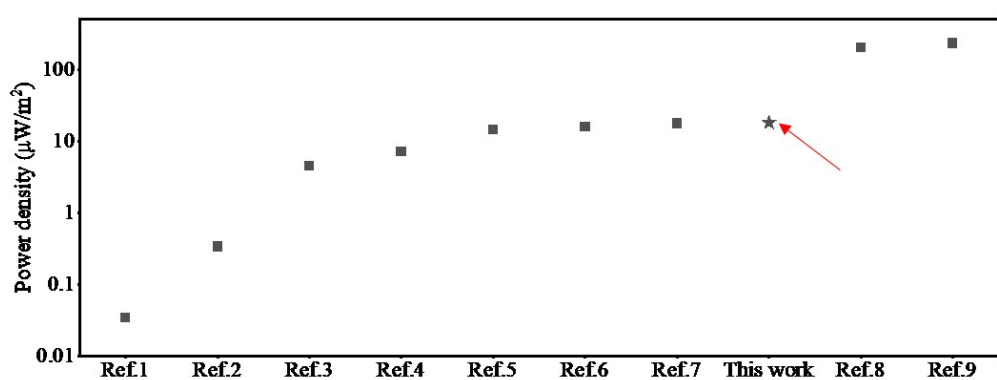


Fig. S14 The output power comparison of generator.

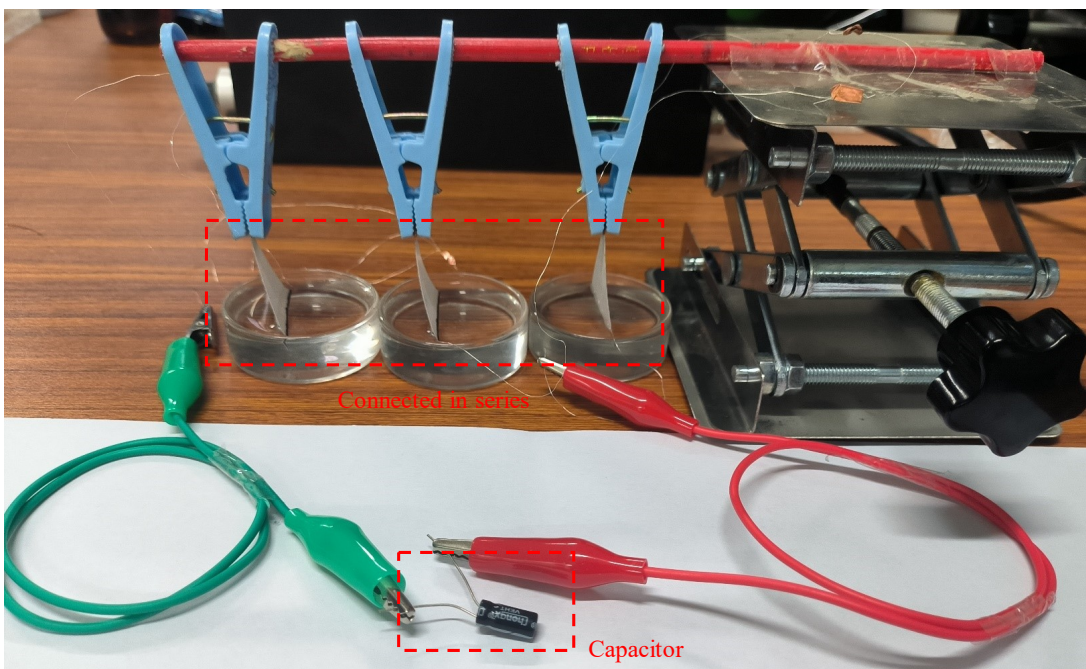


Fig. S15 The real optical image of PTFE membrane charging capacitor.

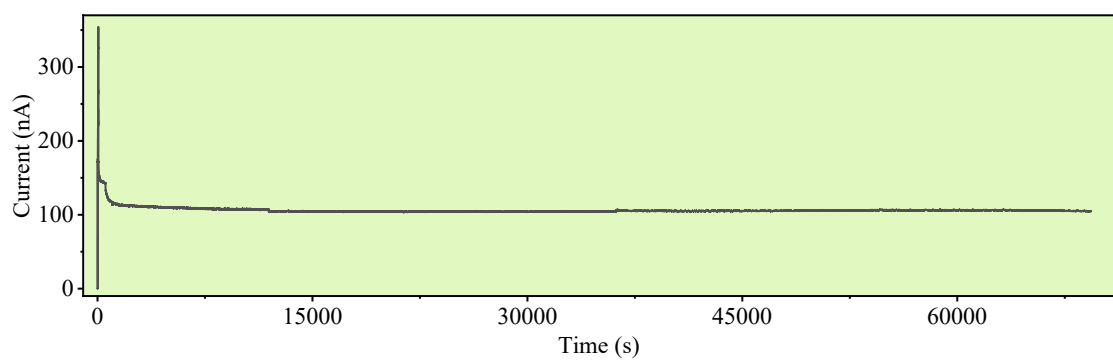


Fig. S16 The stability test of short circuit current.

References

- [1] J.Y. Park, Y. Kwak, J.-E. Lee, Y.-D. Kim, S.-H. Lee, D.-W. Jeong, B.-S. Kim, Y.-H. Choa, Hydrovoltaic electricity generator using a hierarchical NiFe LDH-coated CuO nanowire mesh device, *Chem. Eng. J.* 485 (2024) 149914.
- [2] Y. Xu, J. Xu, J. Zhang, X. Li, B. Fu, C. Song, W. Shang, P. Tao, T. Deng, All-in-one polymer sponge composite 3D evaporators for simultaneous high-flux solar-thermal desalination and electricity generation, *Nano Energy* 93 (2022) 106882.
- [3] Y. Zhang, T. Xiong, L. Suresh, H. Qu, X. Zhang, Q. Zhang, J. Yang, S.C. Tan, Guaranteeing Complete Salt Rejection by Channeling Saline Water through Fluidic Photothermal Structure toward Synergistic Zero Energy Clean Water Production and In Situ Energy Generation, *ACS Energy Lett.* 5 (2020) 3397–3404.
- [4] W. Yang, X. Li, X. Han, W. Zhang, Z. Wang, X. Ma, M. Li, C. Li, Asymmetric ionic aerogel of biologic nanofibrils for harvesting electricity from moisture, *Nano Energy* 71 (2020) 104610.
- [5] J. Zhang, P. Cui, J. Wang, H. Meng, Y. Ge, C. Feng, H. Liu, Y. Meng, Z. Zhou, N. Xuan, B. Zhang, G. Cheng, Z. Du, Paper-Based Hydroelectric Generators for Water

Evaporation-Induced Electricity Generation, *Adv. Sci.* 10 (2023) 2304482.

- [6] Z. Wang, Y. Wu, K. Xu, L. Jiang, J. Sun, G. Cai, G. Li, B.Y. Xia, H. Liu, Hierarchical Oriented Metal–Organic Frameworks Assemblies for Water-Evaporation Induced Electricity Generation, *Adv. Funct. Mater.* 31 (47) (2021) 2104732.
- [7] F. Gao, J. Tu, J. Qu, J. Ge, Q. Yin, Y. Zang, W. Zhong, Z. Jiao, Dual mechanisms based on synergistic effects of evaporation potential and streaming potential for natural water evaporation, *J. Colloid Interface Sci.* 663 (2024) 251–261.
- [8] S.-H. Lee, H.-W. Lee, S.H. Baek, J. Yun, Y. Kwon, B.S. Kim, Y.-H. Choa, D.-W. Jeong, Water-Based Generators with Cellulose Acetate: Uncovering the Mechanisms of Power Generation, *Polymers* 16 (2024) 433.
- [9] W. Deng, G. Feng, L. Li, X. Wang, H. Lu, X. Li, J. Li, W. Guo, J. Yin, Capillary front broadening for water-evaporationinduced electricity of one kilovolt, *Energy Environ. Sci.* 16 (2023) 4442–4452.